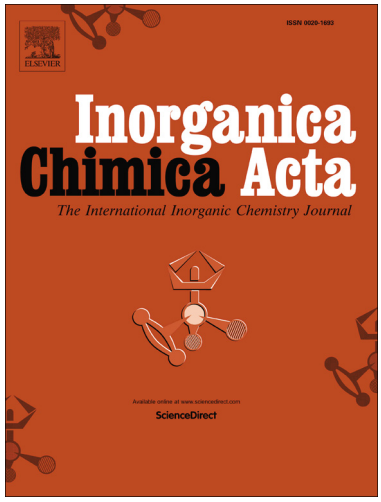

Second generation O-alkyldithiocarbonates: Easy access to a new class of metalloligands

Radu F. Semeniuc , .Thomas J. Reamer, Kaitlyn A. Hammock, Holly B. Jones, Mark D. Smith, Kraig A. Wheeler

PII: S0020-1693(17)30939-8
DOI: http://dx.doi.org/10.1016/j.ica.2017.08.062
Reference: ICA 17859

To appear in: *Inorganica Chimica Acta*

Received Date: 22 June 2017
Revised Date: 27 August 2017
Accepted Date: 31 August 2017

Please cite this article as: R.F. Semeniuc, ..J. Reamer, K.A. Hammock, H.B. Jones, M.D. Smith, K.A. Wheeler, Second generation O-alkyldithiocarbonates: Easy access to a new class of metalloligands, *Inorganica Chimica Acta* (2017), doi: http://dx.doi.org/10.1016/j.ica.2017.08.062

Second generation O-alkyldithiocarbonates: Easy access to a new class of metalloligands

Radu F. Semeniuc,[a,]* Thomas J. Reamer,[a] Kaitlyn A. Hammock,[a] Holly B. Jones,[a] Mark D. Smith,[b] and Kraig A. Wheeler[a]

[a] Department of Chemistry and Biochemistry, Eastern Illinois University, Charleston, IL 61920, USA.
[b] Department of Chemistry and Biochemistry, University of South Carolina, Columbia, SC 29208, USA.

Corresponding author:
Radu F. Semeniuc
Department of Chemistry, Eastern Illinois University
Charleston, IL 61920, USA.
Tel: +1 217 581 5422; E-mail: rsemeniuc@eiu.edu

Dedicated to Professor Ionel Haiduc on the occasion of his 80th birthday. R. F. Semeniuc wishes to express his gratitude to Professor Ionel Haiduc for outstanding guidance during his undergraduate and graduate studies at Babes-Bolyai University, Chemistry Department.

Abstract

The second-generation xanthate ligand 4-$PyCH_2OCS_2Na$, consisting of a backbone functionalized O-alkyldithiocarbonate donor set, has been prepared. The reaction of this ligand with either Ph_3SnCl or $(Ph_3P)_2CuNO_3$ yields the neutral monometallic complexes [4-$PyCH_2OCS_2SnPh_3$] and [4-$PyCH_2OCS_2Cu(PPh_3)_2$], respectively. These compounds were characterized by ^{1}H-NMR and UV-Vis spectroscopies, and in solid state by single crystal X-ray diffraction. The structure of [4-$PyCH_2OCS_2SnPh_3$] consists of a mono-dimensional coordination polymer, formed by the monodentate coordination of the -O-CS_2^- group to the Sn(IV) center, in combination with the coordination of the pyridine group to an adjacent tin atom. In the case of [4-$PyCH_2OCS_2Cu(PPh_3)_2$], the xanthate ligand coordinates to the Cu(I) center in an isobidentate fashion, leaving the pyridine moiety free. These monometallic complexes act as metalloligands toward the $[Rh_2(OAc)_4]$ dimer, producing the tetrametallic derivatives $[Rh_2(OAc)_4]\cdot 2$[4-$PyCH_2OCS_2SnPh_3$] and $[Rh_2(OAc)_4]\cdot 2$[4-$PyCH_2OCS_2Cu(PPh_3)_2$], respectively. These compounds were investigated in solution phase using ^{1}H-NMR and UV-Vis techniques, and it is proposed that the formation of the first compound proceeds *via* a two-step process, while the formation of the latter is a one-step process.

Keywords: O-Alkyldithiocarbonates; X-ray crystal structures; Tin complexes; Copper complexes; Supramolecular Chemistry.

Highlights:

- A backbone functionalized xanthate ligand has been prepared.
- Its propensity to coordinate to Sn(IV) and Cu(I) centers has been explored.
- Neutral metalloligands have been obtained.
- Hetero-tetrametallic complexes have been prepared.

1. Introduction

A major direction that has emerged within chemical research around the world involves applying the principles of supramolecular chemistry in a quest for new materials with useful properties. Promising results have been accomplished and startling applications are being developed by preparing well-defined, self-assembled superstructures with specific properties [1]. Organizational control is achieved by incorporating specific recognition sites within the structures of the building blocks that will drive the self-assembling process toward the desired goal. Dative bonds [2], secondary bonds [3], hydrogen bonding [2e, 4], and π–π stacking [2e, 5] are among the most frequently employed interactions to organize a large variety of building blocks into higher-order arrays.

In this context, the development of new materials based on polynuclear metal complexes witnessed an increased attention during the last years. Numerous compounds, ranging from discrete homo- and/or hetero-nuclear architectures to metal-organic-frameworks with various topologies have been prepared and characterized [6]. One of the most employed synthetic strategies in the preparation of these materials utilizes metal complexes supported by ligands possessing additional functional groups that would allow the expansion of the building blocks into the desired extended structure [7]. These species (also known as metalloligands) are generated by a ligand having at least two donor sites: one for binding to a primary metal ion in a first step, and the other(s) for subsequent coordination to additional metal center(s). In the resulting architecture, the metal ions play two essential functions: a structural task, by directing and supporting the solid-state architecture and a functional role, by bringing desired properties into the final network [8].

To ensure the stability of the metalloligand and avoid the competition between the metal ions during the subsequent steps, most of the metalloligands prepared to date were built around hard, chelating donor groups such as catecholate, acetylacetonate, porphyrin, and Schiff-base scaffolds [6b]. These primary coordination sites deliver relatively non-labile complexes; furthermore, these moieties can be easily modified at several positions with additional rigid functionalities, thus offering a high degree of predictability of the resulting polymetallic architectures.

Soft 1,1-dithiolates ($-ES_2^-$, E = C or P), such as dithiocarbamates ($R_2NCS_2^-$), O-alkyldithiocarbonates ($ROCS_2^-$), and phosphor-1,1-dithiolates ($R[R']PS_2^-$, $R[OR']PS_2^-$, and $RO[R'O]PS_2^-$) represent an important family of ligands that present both practical and academic interest [3e, 3f, 9]. Surprisingly, in spite of years of chemistry, there are only a few reports on the incorporation of soft 1,1'-dithiolate ligands into polyfunctional systems as a means to design heterometallic species [10-12]. Only recently, the Beer group used the dithiocarbamate donor set to prepare supramolecular architectures such as macrocycles, cages, catenanes, and resorcinarene-based assemblies [10]. Wilton-Ely prepared piperazine-based ditopic dithiocarbamate ligands and used them in the preparation of catalytically active homo- and hetero polymetallic species [11]. Polytopic dithiocarbamates were also used in the synthesis of diorganotin-based cavitands and capsules [12]. These examples clearly demonstrate the potential of 1,1'-dithiolates to support complex molecular edifices when combined with other "supramolecular functionalities". While the use of bridging ligands to tether together the same or different metallic centers has been ongoing for several years, the self-assembly of heterometallic architectures built on heteroditopic ligands incorporating the $-ES_2^-$ donor set represents a promising research area that has not been yet exploited to its full potential.

O-alkyldithiocarbonate ligands (also known as xanthates) and their metal complexes have been extensively studied. Following the pioneering work of Hoskins and Winter [9a, 9b, 13], systematic structural analyses performed by Haiduc and Tiekink showed that these ligands can bind to metal centers in a variety of coordination modes, as pictured in Scheme 1 [9f]. In addition, the rich structural features of their metal complexes stem from the presence of the soft Lewis acidic centers on these ligands (*i.e.* sulfur), thus offering the possibility of supramolecular association in the crystalline phase through hypervalent interactions and/or secondary bonds [9e, 9f].

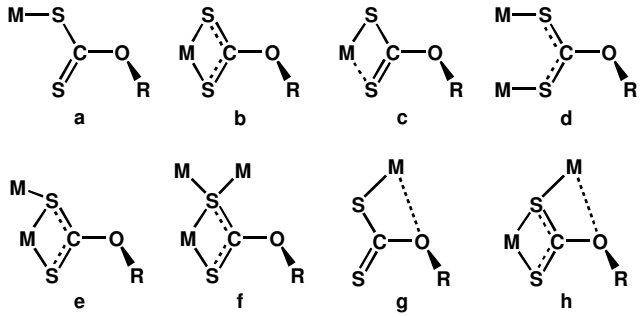

Scheme 1. Coordination modes of the xanthate ligands: a) monodentate; b) isobidentate; c) anisobidentate; d) bimetallic biconnective; e) bimetallic triconnective; f) trimetallic tetraconnective; g) bimetallic biconnective with oxygen involvement; h) bimetallic tetraconnective with oxygen involvement.

Given the scarce number of reports in the literature on xanthate ligands functionalized with additional donor groups that would expand their coordination capabilities [14], we have started a project aimed at the synthesis of "second-generation" O-alkyldithiocarbonate ligands (that is backbone-functionalized xanthates) and their corresponding metal complexes.

By attaching to the backbone of the soft -O-CS_2^- donor set other moieties with coordination capabilities (for instance donors such as pyridine-based groups), it should be possible to take advantage of the differences between the coordination preferences of sulfur atoms for "soft metals" and of pyridine-based groups for other metals to design and prepare new heterometallic species. First, the negatively charged -CS_2^- group would selectively accept a suitable metal system at the "soft end" of the ligand through a charge assisted process, while keeping the pyridine end free for further coordination opportunities. Next, additional coordinatively unsaturated metal centers would connect to the resulting metalloligand, generating the desired heterometallic complexes.

Following this strategy, we have prepared our first second-generation xanthate ligand, 4-$PyCH_2OCS_2Na$ and reported its use in the preparation of a luminescent $[CH_3OCH_2CH_2OP(An)S_2]_2Ni{\cdot}2[(4\text{-}PyCH_2OCS_2)Re(bipy)(CO)_3]$ (An = anisole) trinuclear complex, supported by a heteroleptic xanthate-dithiophosphonate ligand system [15]. In this contribution, we wish to report a more detailed characterization of this ligand, as well as its use in the preparation of two new metalloligands incorporating Sn(IV) and Cu(I) metallic centers. Also reported here is the use of these metalloligands in the preparation of tetranuclear Rh(II) – Sn(IV) and Rh(II) – Cu(I) heterometallic complexes.

2. Results and Discussion

2.1. Syntheses and characterization

The syntheses of the second-generation xanthate ligand, its corresponding Sn(IV) and Cu(I) metalloligands and the tetranuclear Rh(II) based heterometallic complexes are depicted in Scheme 2. The 4-$PyCH_2OCS_2Na$ ligand was prepared in excellent yields as reported [15], by deprotonating 4-pyridine-methanol with NaH in dry THF, followed by the CS_2 reaction with the formed sodium alkoxide. The ligand is stable for several weeks in air, soluble in water, alcohols, and acetone, and insoluble in halogenated solvents and ethers. The reaction of 4-$PyCH_2OCS_2Na$ with either Ph_3SnCl or $(Ph_3P)_2CuNO_3$ yields [4-$PyCH_2OCS_2SnPh_3$] (**[Py-Sn]**) and [4-$PyCH_2OCS_2Cu(PPh_3)_2$] (**[Py-Cu]**), respectively. Both compounds are air and moisture stable powders, and soluble in common organic solvents, but insoluble in alcohols, ethers, and water. The reaction of two equivalents of **[Py-Sn]** and **[Py-Cu]** metalloligands with one equivalent of $[Rh_2(OAc)_4]\cdot 2MeOH$ dimer in acetone yields the tetrametallic derivatives $[Rh_2(OAc)_4]\cdot 2[4\text{-}PyCH_2OCS_2SnPh_3]$ (**[Rh]-2[Py-Sn]**) and $[Rh_2(OAc)_4]\cdot 2[4\text{-}PyCH_2OCS_2Cu(PPh_3)_2]$ (**[Rh]-2[Py-Cu]**), respectively. While the Sn(IV)-based complex is soluble in common organic solvents, its Cu(I) congener shows a very low solubility in the same solvents.

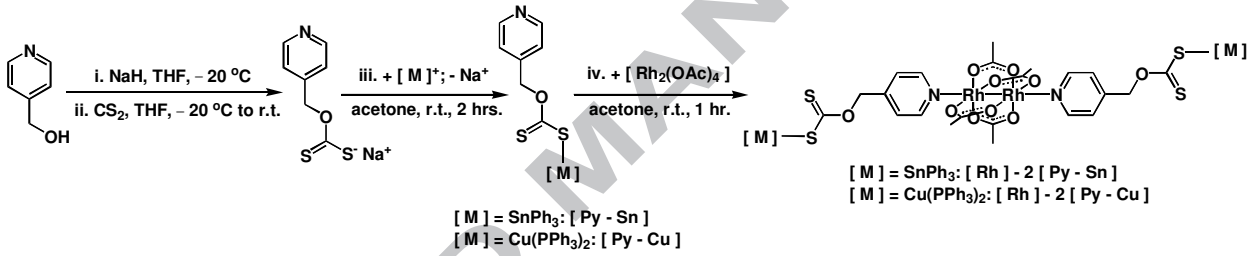

Scheme 2. The synthesis of Rh-based tetranuclear heterometallic complexes supported by the second-generation 4-$PyCH_2OCS_2Na$ ligand *via* its corresponding Sn(IV) and Cu(I) metalloligands.

The ^{1}H-NMR spectra (acetone-d_6) of the synthesized compounds are pictured in Fig. 1. The formation of the 4-$PyCH_2OCS_2Na$ ligand from 4-$PyCH_2OH$ is evident, as the -CH_2- peak is shifted downfield, from 4.71 ppm to 5.59 ppm, due to the CS_2 insertion. As expected, the pyridine signals are not affected by the presence of the O-alkyldithiocarbonate group (see Fig. 1 a and b).

Upon coordination of the -O-CS_2^- group to Sn(IV) and Cu(I) centers, the ^{1}H-NMR spectra clearly shows the formation of the corresponding metalloligands (Fig. 1 c and e). For **[Py-Sn]** the characteristic Ph_3Sn peaks appear as multiplets in the 7.77-7.62 ppm and 7.54-7.44 ppm intervals, while for **[Py-Cu]** the $(Ph_3P)_2$Cu signals appear between 7.49 and 7.25 ppm. Further, in the case of the **[Py-Sn]** complex (see Fig. 1b and Fig. 1c), the pyridine peaks experience a significant shift (from 8.51 to 8.41 ppm ($\Delta\delta$ = 0.1 ppm) and from 7.35 to 6.91 ppm ($\Delta\delta$ = 0.44 ppm)), suggesting the coordination of the pyridine group to the tin centers. In contrast, upon the formation of the **[Py-Cu]** complex, the pyridine peaks do not shift from their original position in 4-$PyCH_2OCS_2Na$ (8.58 ppm vs. 8.51 ppm; the second pyridine signal overlap with those from the Ph_3P moieties, but they are in the 7.49-7.25 ppm range, close to the original position of 7.35 ppm in the ligand – compare Fig 1b with Fig. 1e).

The pyridine peaks of the tetrametallic **[Rh]-2[Py-Sn]** derivative (Fig. 1 d) are shifted downfield when compared to the same peaks of the **[Py-Sn]** metalloligand (from 8.41 to 9.11 ppm ($\Delta\delta$ = 0.7 ppm) and

from 6.91 to 7.29 ppm ($\Delta\delta$ = 0.38 ppm)), indicative of pyridine coordination to the Rh centers. In the case of **[Rh]-2[Py-Cu]** derivative, the low solubility of this complex in acetone precludes a detailed analysis; however, its NMR spectrum (Fig. 1 f) suggests the formation of the desired tetrametallic derivative.

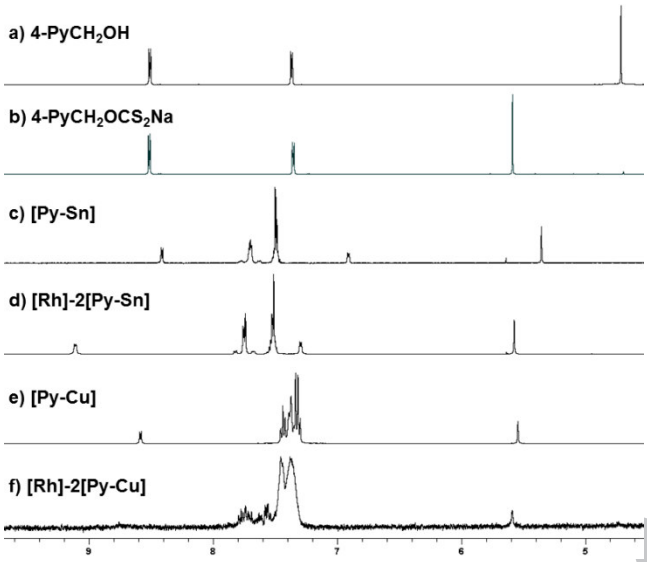

Fig. 1. Partial ^{1}H-NMR spectra (acetone-d_6) of a) 4-PyCH$_2$OH; b) 4-PyCH$_2$OCS$_2$Na; c) **[Py-Sn]**; d) **[Rh]-2[Py-Sn]**; e) **[Py-Cu]**; f) **[Rh]-2[Py-Cu]**.

2.2. Solid state studies

Single crystals of 4-PyCH$_2$OCS$_2$Na, **[Py-Sn]**, and **[Py-Cu]** were grown by vapor phase diffusion of diethyl ether into acetone solutions of the compounds and subjected to X-ray diffraction studies. Crystal data and structure refinement details are collected in Table 1 and selected bond lengths and angles are listed in Table 2.

2.2.1. Structural characterization of 4-PyCH$_2$OCS$_2$Na

The binding mode of 4-PyCH$_2$OCS$_2$Na and the coordination environment around the sodium ion are pictured in Fig. 2. The -O-CS$_2^-$ group alone shows an unusual trimetallic pentaconnective coordination mode. If we also consider the pyridine group positioned at the backbone of the -O-CS$_2^-$ donor set, the 4-PyCH$_2$OCS$_2^-$ moiety acts as a bridging ligand, binding the Na ion in a tetrametallic hexaconnective fashion.

The "classic" -O-CS$_2^-$ donor set chelates one Na ion in a partial anisobidentate mode (S1-Na1 = 2.930 Å and S2-Na1 = 3.036 Å), the difference between the two S – Na bond lengths being 0.106 Å. In addition, the S1 atom coordinates to two more sodium ions, Na1' and Na1'', the corresponding bond lengths being 2.986 Å and 3.030 Å, respectively. The O atom of the xanthate ligand is also involved in coordination to the metallic center, the O1-Na1' bond length being 2.543 Å. A water molecule is also present, bridging two Na ions, the O2-Na' bond length being 2.476 Å. The pyridine ring of the ligand

coordinates to a third sodium, with a N1-Na1''' bond length of 2.468 Å. Overall, the geometry around the Na1 center can be described as a distorted pentagonal bipyramid. The equatorial positions are occupied by the S1, S2, S1''', O2', and O1'', and the axial positions by the N1'' and S1'''' atoms. The average N1''-Na1-equatorial atoms angle is 93.94°, while the average S1''''-Na1-equatorial atoms angle is 85.93°, and the N1''-Na1-S1'''' angle is 166.66°. The bridging feature of the water molecule imposes the largest distortion from the ideal geometry, the N-Na-O2 and S-Na-O2 angles being 120.13° and 73.20°, respectively.

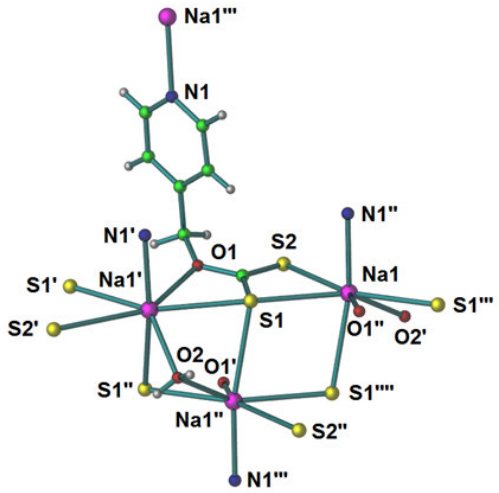

Fig. 2. Binding mode and coordination environment around the sodium center in 4-PyCH$_2$OCS$_2$Na.

This coordination mode of the ligand generates an undulating inorganic $(Na_2S_2)_\infty$ ladder (see Fig. 3), running along the *c* axis of the unit cell. This arrangement consist of two types of alternating Na-S-Na-S metallacycles, one made by the coordination of S1 atom to the Na1 and Na1' centers (and the symmetry related S1' atom to the same sodium ions), and the other by the S1' and S1'' coordination to the Na1 and Na1'' ions, respectively. The latter metallacycle also contains the bridging water molecule. The Na ⋯ Na distances within the ladder fall in the range from 3.676 Å for the Na1-Na1'' distance, to 4.642 Å for Na1-Na1', and 5.896 Å for Na1'-Na1''. The corresponding angles are S1-Na1-S1' = 77.73° and Na1-S1-Na1' = 102.27° for the first metallacycle, and S1'-Na1-S1'' = 97.01° and Na1-S1'-Na1'' = 75.34° for the second. These two metallacycles are connected by the bridging S1 atoms, the S1-Na1-S1'' and Na1'-S1'-Na1'' angles being 141.35° and 170.52°, respectively.

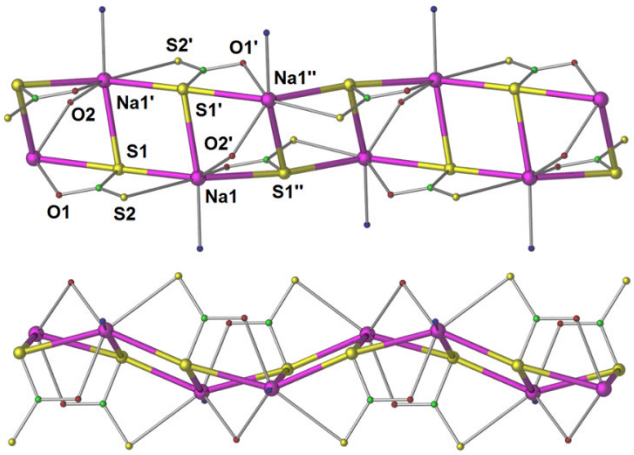

Fig. 3. Two views of the Na_2S_2 inorganic ladder in 4-$PyCH_2OCS_2Na$.

As described above, each Na^+ ion is also coordinated by the pyridine ring of the xanthate ligand. Due to the bridging nature of the ligand, the overall structure of the 4-$PyCH_2OCS_2Na$ complex consists of a three-dimensional architecture, as pictured in Fig. 4. As each Na center is coordinated by one pyridine moiety, the -O-CS_2^- group (oriented in the opposite direction of the coordinate vector of the N_{py} atom) participates in the formation of additional Na_2S_2 ladders, all connected by the ligand in an overall W-shaped structure.

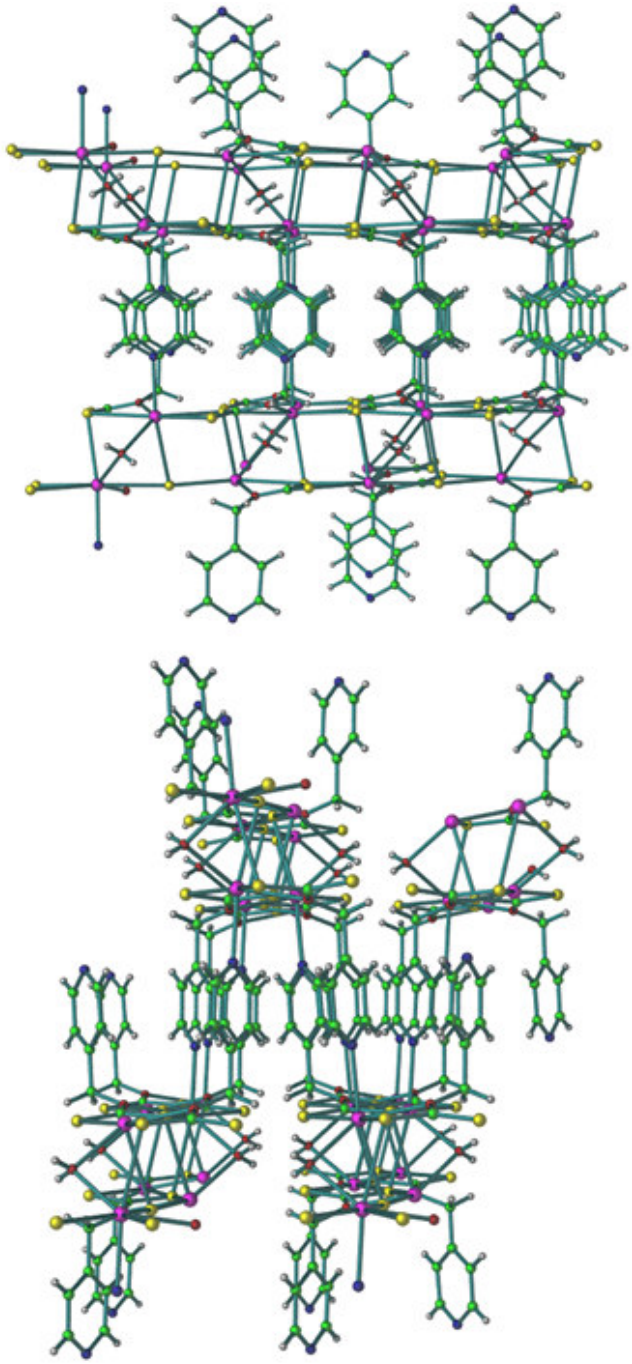

Fig. 4. The three-dimensional structure of the 4-$PyCH_2OCS_2Na$ complex.

*2.2.2. Structural characterization of [4-$PyCH_2OCS_2SnPh_3$] (**[Py-Sn]**)*

The coordination environment around the tin atom in **[Py-Sn]** is pictured at the top of Fig. 5. The xanthate ligand binds to the Sn(IV) center in a monodentate fashion (S1-Sn1 = 2.593 Å), with the second sulfur atom of the -O-CS_2^- group oriented away from the metal. This monodentate coordination mode is

reflected in the different C-S bond lengths, their values (1.724 Å for C1-S1 and 1.648 Å for C1-S2) suggesting some delocalization of the carbon – sulfur double bond. The oxygen atom of the ligand is oriented toward the tin atom, but the O ⋯ Sn distance of 3.179Å does not suggest a significant interaction between these two atoms. The Sn(IV) center is equatorially surrounded by the phenyl groups, with a C-Sn bond length average of 2.135 Å. Interestingly, the pyridine atom of the ligand is also involved in coordination, binding to a tin atom from an adjacent 4-$PyCH_2OCS_2SnPh_3$ unit. As such, the geometry around the tin center can be described as distorted trigonal bipyramid. In the case of five-coordinated complexes, which can have either a trigonal bipyramidal or a square pyramidal geometry, the degree of distortion from the ideal geometry is described by the angular parameter τ_5 [16]. This parameter is calculated by dividing the difference between the two largest angles by 60; a trigonal bipyramidal structure would produce a value of 1, while a square pyramidal structure would produce a value of 0. For this complex, the τ_5 value is 0.7, clearly indicating a distortion from the ideal trigonal bipyramidal geometry.

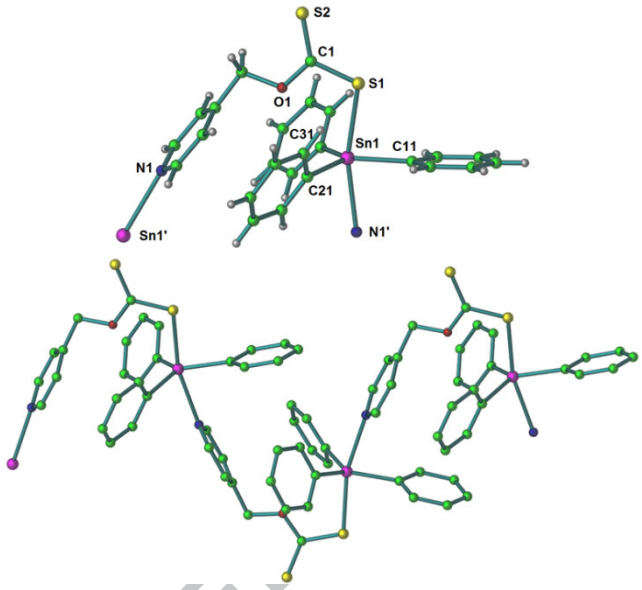

Fig. 5. The coordination environment around the Sn(IV) center (top) and the mono-dimensional coordination polymer **[Py-Sn]**$_\infty$ (bottom).

The binding of the pyridine ring to the Sn(IV) atom leads to the formation of a mono-dimensional coordination polymer, depicted at the bottom of Fig. 5. The -O-CH_2- spacer is bent over the Ph_3Sn group, placing the pyridine ring in close proximity of two of the three phenyl rings attached to the tin center. Another phenyl ring, from an adjacent Ph_3Sn moiety, also points toward the pyridine and phenyl rings. Although several carbon – carbon distances are below 3.8 Å, the orientation of these aromatic regions do not support the existence of C-H⋯π or π-π stacking interactions.

*2.2.3. Structural characterization of [4-$PyCH_2OCS_2Cu(PPh_3)_2$] (**[Py-Cu]**)*

The molecular structure of **[Py-Cu]** is depicted in Fig. 6. There are two crystallographically independent molecules per asymmetric unit, both having the same structural features, with only small

differences between their bond lengths and angles (see Table 2); therefore, only one molecule will be described here. The -O-CS_2^- end of the ligand coordinates to the Cu(I) center in an essentially isobidentate mode with the two S – Cu bond lengths practically equal at S1A-Cu1 = 2.390 Å and S2A-Cu1 = 2.427 Å, respectively. The C1A-S1A and C1A-S2A bond lengths, nearly equal at 1.696 Å and 1.689 Å, respectively, also support this fact. The coordination sphere around the metal is filled by two PPh_3 moieties, with P1A-Cu1 and P2A-Cu1 bond lengths of 2.246 Å and 2.233 Å, respectively. The metal center is in a distorted tetrahedral environment, distortion imposed by the "bite" angle of the xanthate ligand, the S1A-Cu1-S2A angle being 75.31°. The most important feature of this complex is the fact that the pyridine group is not involved in the coordination of the ligand to the Cu(I) ion, thus remaining available to bind to a second metallic center.

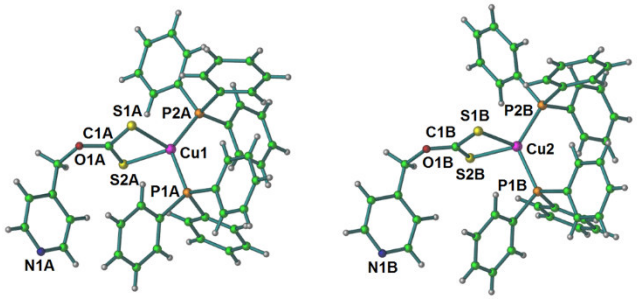

Fig. 6. The molecular structures of the two independent **[Py-Cu]** molecules.

2.3. Solution studies

As described above, the 4-PyCH_2OCS_2Na ligand produces the **[Py-Sn]** and **[Py-Cu]** complexes, mainly distinguished by the behavior of the pyridine ring: while in the first complex the Py moiety acts as a donor group, in the latter it is not coordinated to the metal center. Considering the above results, two questions immediately rise: can these metalloligands coordinate to additional metallic centers to form heterometallic complexes and, in the case of **[Py-Sn]**, how would the formation of a heterometallic complex (if possible at all) be influenced by the coordination of the N_{py} atom to the Sn(IV) centers? To answer these questions in the absence of crystallographic evidence for the formation of the dirhodium-based tetrametallic complexes, we investigated the interaction between our metalloligands and the dirhodium tetraacetate complex in solution phase.

In the $[Rh_2(OAc)_4]\cdot 2MeOH$ starting material, the acetates are kinetically inert and they can be exchanged only in harsh conditions. In contrast, the methanol molecules (or any other axial donor ligands like acetone or water) are labile, and can be easily exchanged with stronger σ-donor ligands. The electronic properties of the dirhodium tetraacetate dimer offer a unique possibility to study its interaction with the **[Py-Sn]** and **[Py-Cu]** metalloligands. Scheme 3 depicts a qualitative MO diagram for a dirhodium tetraacetate dimer of the general formula $[Rh_2(OAc)_4]L_2$ (where L is the axial ligand), built from a $[Rh_2(OAc)_4]$ dimer (D_{4h} overall symmetry) and two axial σ-donor ligands [17]. The σ-donor lone pairs of the axial L ligands have two symmetry combinations, a_{1g} and a_{2u}. While the a_{1g} combination will stabilize the Rh-Rh σ bonding orbital, the a_{2u} combination will raise the energy of the Rh-Rh σ* LUMO. One of the consequences of this increase in energy is the change in the energy of the lowest energy absorption in dirhodium complexes, the e_g π* → a_{2u} σ* HOMO-LUMO transition, leading to a shift of the

λ_{max}, depending on the nature of the axial ligands. For example, in the case of $Rh_2(TIPB)_4$ (TIPB = 2,4,6-triisopropylbenzoate), a dirhodium tetracarboxylate complex that can be isolated without axial ligands, addition of different (axial) ligands like water or acetone, changes the λ_{max} from 760 nm in the "free" complex to 670 nm for water, and to 610 nm for acetone [18].

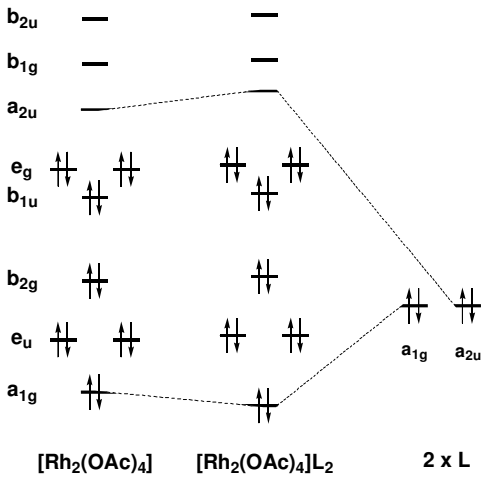

Scheme 3. Qualitative molecular orbital diagram for a $[Rh_2(OAc)_4]L_2$ complex; redrawn from ref. [17].

The titration of $[Rh_2(OAc)_4]$ with increasing amounts of **[Py-Sn]** (in 0.2 equivalent increments, up to 3.0 equivalents) was carried out in a 1 : 1 acetone – dichloromethane mixture and followed spectrophotometrically, by monitoring the λ_{max} shift of the lowest energy absorption, see Fig. 7. As more equivalents of **[Py-Sn]** are added, the λ_{max} shifts from 600 nm (the blue line in Fig. 7 – corresponding to the "uncoordinated" dirhodium complex) to 532 nm (the purple line in Fig. 7 – corresponding to 3 equivalents of **[Py-Sn]** added to the bimetallic center).

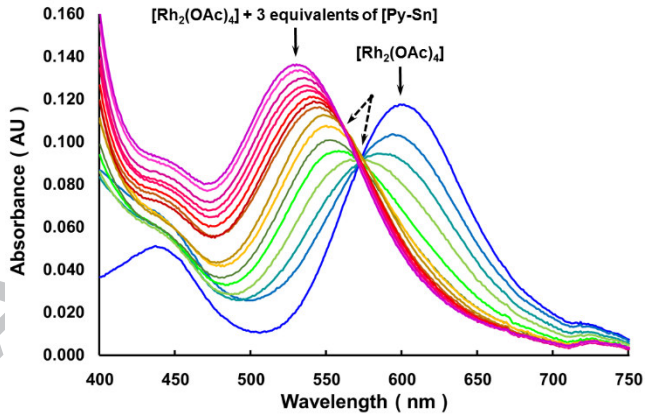

Fig. 7. Absorption spectra collected during the titration of $[Rh_2(OAc)_4]$ with **[Py-Sn]**; the dashed arrows point toward two isosbestic points identified during the titration experiment.

We attempted to perform a similar experiment using the **[Py-Cu]** metalloligand. Unfortunately, a detailed study was hampered not only by the low solubility of the **[Rh]-2[Py-Cu]** complex in the reaction

media, but also by the tail of a strong absorption of the complex in the UV region, overlapping with the absorptions in the visible region. As it can be seen in Fig. 8, we were able to add only 0.7 equivalents (in 0.1 increments) of **[Py-Cu]** to the dirhodium center; the addition of one more 0.1 equivalent of **[Py-Cu]** to **[Rh]** made any reading of the λ_{max} value impossible.

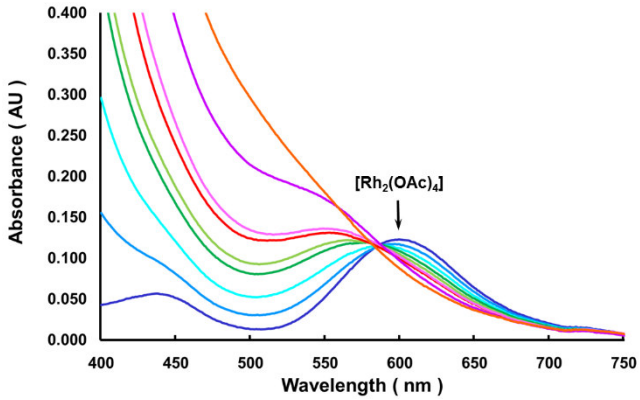

Fig. 8. Absorption spectra collected during the titration of $[Rh_2(OAc)_4]$ with **[Py-Cu]**.

These experiments provided some insight into the solution structure of the complexes. To confirm the 1 : 2 stoichiometry of our tetrametallic complexes, we chose the Yoe-Jones' mole-ratio method, which consists of analyzing a series of solutions in which the concentration of one reactant is kept constant, while increasing the concentration of the other reactant [19]. By plotting the change in a property of the complex (in this case the change in λ_{max}) against the mole-ratio of the two reactants, in addition to finding the stoichiometry of a complex, one can also identify if the formation of a ML_2 complex proceeds directly or if it is a stepwise process. The results of these investigations are shown in Fig. 9. In the case of the **[Rh]-2[Py-Sn]** system, the titration curve is indicated by the blue dots. As more and more equivalents of **[Py-Sn]** are added, the λ_{max} shifts to lower wavelengths, until 1.0 equivalent of metalloligand is present in solution, when the λ_{max} value is 552 nm. Upon addition of 1.2 equivalents or more of **[Py-Sn]** to $[Rh_2(OAc)_4]$, a change in the slope is observed, but only up to 2.0 equivalents of **[Py-Sn]** (the corresponding λ_{max} value being 543 nm), when another change in the variation of λ_{max} values becomes evident. Addition of more metalloligand leads to a flatlining behavior at λ_{max} = 532 nm, suggesting the saturation of the system. These data imply that the formation of the **[Rh]-2[Py-Sn]** complex proceeds stepwise, according to equations (1) and (2).

This stepwise process is also supported by a close inspection of the spectra of the **[Rh]-2[Py-Sn]** system, which reveals the presence of two well-defined isosbestic points, shown by the dashed lines in Fig. 7. Nevertheless, these two points do not appear simultaneously. The first isosbestic point (positioned around 571 nm) is produced only by the first six spectral lines, corresponding to 0.0, 0.2, 0.4, 0.6, 0.8, and 1.0 equivalents of **[Py-Sn]** added to the rhodium starting material. The second point, located around 561 nm is formed by the intersection of the remaining spectral lines, from 1.2 to 3.0 equivalents of **[Py-Sn]** added to the system. This suggests that during the titration process two absorbing species are present in solution, *e.g.* the $[Rh_2(OAc)_4]$ and the **[Rh]-[Py-Sn]** complexes in the first step of the reaction, and the **[Rh]-[Py-Sn]** and **[Rh]-2[Py-Sn]** complexes in the second step, respectively.

For the reasons mentioned above (low solubility of the compound and overlapping absorption bands), we were not able to gather sufficient data points to investigate the $[Rh_2(OAc)_4]$ / **[Py-Cu]** system in detail. The available seven data points (shown as purple squares in Fig. 9) show a dramatic change in the λ_{max}

values ($\Delta\ \lambda_{max}$ = 62 nm, from 600 nm to 538 nm), even after the addition of only 0.7 equivalents of metalloligand. This suggests that the formation of **[Rh]-2[Py-Cu]** complex is a one step process, as shown in equation (3).

To identify the λ_{max} value for a 1 : 2 Rh : pyridine-based ligand complex, we added an excess of 4-picoline to the dirhodium starting material, yielding a soluble **[Rh]-2[4-picoline]** compound. Its absorption spectrum displays a λ_{max} value at 520 nm, close to the one shown by our **[Rh]-2[Py-Cu]** complex (538 nm), suggesting that the addition of 0.7 equivalents of **[Py-Cu]** produces directly the desired Rh-Cu tetrametallic derivative. However, in the absence of more data points, we can only speculate on the processes taking place within the $[Rh_2(OAc)_4]$ / **[Py-Cu]** system.

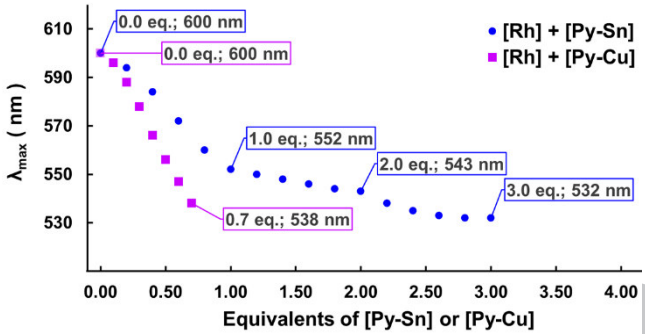

Fig. 9. Plot of the λ_{max} shift against the number of **[Py-Sn]** and **[Py-Cu]** equivalents added to **[Rh]**.

[Rh] + [Py-Sn] ⇌ **[Rh]-[Py-Sn]** **(eq. 1)**

[Rh]-[Py-Sn] + [Py-Sn] ⇌ **[Rh]-2[Py-Sn]** **(eq. 2)**

[Rh] + 2 [Py-Cu] ⇌ **[Rh]-2[Py-Cu]** **(eq. 3)**

3. Conclusions

We have described here a simple, high-yield, stepwise approach toward heterometallic complexes, based on a second-generation, pyridine functionalized xanthate ligand. We have shown that the 4-$PyCH_2OCS_2Na$ ligand binds to Sn(IV) and Cu(I) centers to form metalloligands, that can further react with coordinatively unsaturated metallic centers to produce heterometallic complexes, such as **$[Rh_2(OAc)_4]\cdot 2[4\text{-}PyCH_2OCS_2SnPh_3]$** and **$[Rh_2(OAc)_4]\cdot 2[4\text{-}PyCH_2OCS_2Cu(PPh_3)_2]$**. This approach opens the door toward the synthesis of a large variety of heterometallic architectures, either discrete species (as described here) or extended networks, self-assembled *via* secondary bonds, supported by the various polymetallic-polyconnective coordination modes of the $-O-CS_2^-$ donor group, as will be addressed in forthcoming manuscripts from our group.

4. Experimental

General considerations: Unless otherwise noted, all operations were performed in ambient atmosphere. Operations requiring inert (nitrogen) atmosphere were carried out using standard Schlenk techniques. Solvents were dried by conventional methods and distilled under a dry N_2 atmosphere immediately prior to use. NMR spectra were recorded using a 400 MHz Bruker Avance FT-NMR Spectrometer. UV-Vis spectroscopic investigations were performed on a Cary 100 Agilent Spectrophotometer. $(Ph_3P)_2CuNO_3$ and $[Rh_2(OAc)_4]\cdot 2MeOH$ were prepared as described in the literature [20, 21]. All other reagents were commercially available and were used without further purification.

4-PyCH$_2$OCS$_2$Na: This compound was prepared following a reported procedure [15]. 4-Pyridylcarbinol (1.09 g, 10 mmol) was dissolved in dry THF (50 mL) and added dropwise to a suspension of NaH (0.24 g, 10 mmol) in dry THF (100 mL) under an inert atmosphere at -20^o C (a salt-ice bath). The mixture was stirred for 20 minutes, then excess carbon disulfide (1.0 mL, 1.6 excess) was added dropwise, and the resulting mixture was stirred for one hour while allowed to return to room temperature. The flask was disconnected from the Schlenk line, and the yellow solution was filtered to remove any solid impurities. The THF was removed under reduced pressure, and the resulting yellow powder was dried under vacuum; the solid (1.93 g, yield 93.1 %) was identified as 4-PyCH$_2$OCS$_2$Na; ^{1}H-NMR (acetone-d_6): δ: 8.51 (d, *J* = 5.9 Hz, 2H, *Py*), 7.35 (d, *J* = 6.0 Hz, 2H, *Py*), 5.59 (s, 2H, Py-C*H*$_2$).

[4-PyCH$_2$OCS$_2$SnPh$_3$] ([Py-Sn]): Ph_3SnCl (0.193 g, 0.5 mmol) was dissolved in CH_2Cl_2 (30 mL), and added to a solution of 4-PyCH$_2$OCS$_2$Na (0.104 g, 0.5 mmol) in acetone (15 mL). The mixture was stirred at room temperature for two hours. The resulting NaCl was removed by filtration, and the clear solution was concentrated under reduced pressure and kept in the refrigerator for two hours. The resulting white solid was isolated by filtration, yielding 0.218 g (81.6 %) of the title compound. Anal. Calcd. for $C_{25}H_{21}NOS_2Sn$: C = 56.20, H = 3.96, N = 2.62. Found: C = 56.50, H = 4.26, N = 3.02. ^{1}H-NMR (acetone-d_6): δ: 8.41 (d, *J* = 6.0 Hz, 2H, *Py*), 7.77-7.62 (m, 6H, *Ph*$_3$Sn), 7.54-7.44 (m, 9H, *Ph*$_3$Sn), 6.91 (d, *J* = 5.6 Hz, 2H, *Py*), 5.35 (s, 2H, Py-C*H*$_2$).

[4-PyCH$_2$OCS$_2$Cu(PPh$_3$)$_2$] ([Py-Cu]): $(Ph_3P)_2CuNO_3$ (0.325 g, 0.5 mmol) was dissolved in acetone (20 mL), and added to a solution of 4-PyCH$_2$OCS$_2$Na (0.104 g, 0.5 mmol) in acetone (20 mL). The mixture was stirred at room temperature for two hours. The resulting $NaNO_3$ was removed by filtration, and the solvent was removed under reduced pressure, yielding a light orange compound (0.322 g, 83.4 %), identified as the title compound. Anal. Calcd. for $C_{43}H_{36}CuNOP_2S_2$: C = 66.87, H = 4.70, N = 1.81. Found: C = 66.51, H = 4.37, N = 1.68. ^{1}H-NMR (acetone-d_6): δ: 8.58 (d, *J* = 5.9 Hz, 2H, *Py*), 7.49-7.25 (m, 32H, *Ph*$_3$P overlap with *Py*), 5.54 (s, 2H, Py-C*H*$_2$).

[Rh$_2$(OAc)$_4$]·2[4-PyCH$_2$OCS$_2$SnPh$_3$] ([Rh]-2[Py-Sn]): **[Py-Sn]** (0.107 g, 0.2 mmol) was added as a solid to an emerald green solution of $[Rh_2(OAc)_4]\cdot 2MeOH$ (0.051 g, 0.1 mmol) in acetone (75 mL) and the mixture was stirred for one hour, producing a pink solution. The solvent was removed under vacuum, yielding 0.135 g (89.4 %) of a pale pink solid. The solid was identified as the title compound. Anal. Calcd. for $C_{58}H_{54}N_2O_{10}Rh_2S_4Sn_2$: C = 46.12, H = 3.60, N = 1.85. Found: C = 46.51, H = 3.42, N = 1.54. ^{1}H-NMR (acetone-d_6): δ: 9.11 (d, *J* = 5.4 Hz, 2H, *Py*), 7.83-7.67 (m, 6H, *Ph*$_3$Sn), 7.56-7.47 (m, 9H, *Ph*$_3$Sn), 7.29 (d, *J* = 5.6 Hz, 2H, *Py*), 5.57 (s, 2H, Py-C*H*$_2$).

[Rh$_2$(OAc)$_4$]·2[4-PyCH$_2$OCS$_2$Cu(PPh$_3$)$_2$] ([Rh]-2[Py-Cu]): **[Py-Cu]** (0.154 g, 0.2 mmol) was added as a solid to an emerald green solution of $[Rh_2(OAc)_4]\cdot 2MeOH$ (0.051 g, 0.1 mmol) in acetone (50 mL) and the mixture was stirred for one hour. During this time, a light orange-red precipitate formed, which was collected on a frit by vacuum filtration, washed with diethyl ether and air-dried, yielding 0.179 g (89.9 %) of the title compound. Anal. Calcd. for $C_{94}H_{84}Cu_2N_2O_{10}P_4Rh_2S_4$: C = 56.83, H = 4.26, N = 1.41.

Found: C = 57.17, H = 3.92, N = 1.78. ^{1}H-NMR (acetone-d_6) (all peaks broad and very weak, no assignments were made): δ: 8.73 (s), 7.74-7.37 (m), 5.59 (s).

Crystallography: For **4-PyCH$_2$OCS$_2$Na** and **[Py-Sn]** X-ray intensity data were measured at 150(2) K on a Bruker SMART APEX diffractometer (Mo Kα radiation, λ = 0.71073 Å) [22]. Raw area detector data frame integration was performed with SAINT+ [22]. Final unit cell parameters were determined by least-squares refinement. An absorption correction based on the multiple measurement of equivalent reflections was applied to the data with SADABS [22]. Direct methods structure solution, difference Fourier calculations and full-matrix least-squares refinement against F^2 were performed with SHELXTL [23]. For **[Py-Cu]** the X-ray data were collected at 100(2) K on a Bruker SMART APEXII CCD diffractometer equipped with Cu-Kα radiation. Intensities were collected using phi and omega scans and were corrected for Lorentz polarization and absorption effects. The *X-SEED* software platform [24], equipped with *SHELXS* and *SHELXL* modules on a PC computer [25], was used for structure solution and refinement calculations, and molecular graphics. The structures were solved by direct methods, and refined by anisotropic full-matrix least-squares for all non-hydrogen atoms.

Titration studies: Stock solutions ($1.5 \cdot 10^{-3}$ M) of **[Rh]**, **[Py-Sn]** and **[Py-Cu**] were prepared in an acetone / dichloromethane (1 / 1, v / v) solvent system. Various volumes of **[Py-Sn]** or **[Py-Cu**], corresponding to the desired number of equivalents, were added to a sample (750 μL) of **[Rh]** in a 1 cm path-length cell. The final sample volume was kept constant at 3.0 mL and, accordingly, the final concentration of **[Rh]** was $3.75 \cdot 10^{-4}$ M. The spectra were recorded in the 800 – 350 nm range.

Acknowledgments

The authors thank Eastern Illinois University for a Council on Faculty Research grant. The Single Crystal Diffractometer at EIU was purchased using funds provided by an NSF-MRI grant (CHE-0722547).

Appendix A. Supplementary Material

CCDC 1556155, 1556156, and 1556157contain the supplementary crystallographic data for this paper. These data can be obtained free of charge from The Cambridge Crystallographic Data Centre via www.ccdc.cam.ac.uk/data_request/cif.

Table 1. Crystal data and structure refinement details for **4-PyCH$_2$OCS$_2$Na** and **[Py-Sn]**, and **[Py-Cu]**.

	4-PyCH$_2$OCS$_2$Na	**[Py-Sn]**	**[Py-Cu]**
Chemical formula	$C_{14}H_{14}N_2Na_2O_3S_4$	$C_{25}H_{21}NOS_2Sn$	$C_{43}H_{36}CuNOP_2S_2$
M_r	432.49	534.24	772.33
Crystal system, space group	Orthorhombic, Pbcn	Monoclinic, Cc	Triclinic, P-1
Temperature (K)	150	150	100
a (Å)	20.9667 (14)	9.9076 (6)	15.7555 (4)
b (Å)	7.7314 (5)	18.6634 (11),	16.1195 (4)
c (Å)	11.1372 (7)	13.2763 (8)	17.4752 (4)
α (°)	90	90	71.275 (1)
β (°)	90	110.986 (1)	87.843 (1)
γ (°)	90	90	62.904 (1)
V (Å^3)	1805.4 (2)	2292.1 (2)	3710.78 (16)
Z	4	4	4
μ (mm^{-1})	0.59	1.31	2.97
Crystal size (mm)	0.42 × 0.38 × 0.30	0.42 × 0.24 × 0.22	0.46 × 0.32 × 0.22
T_{min}, T_{max}	0.863, 1.000	0.817, 1.000	0.558, 0.753
No. of measured, independent and observed [I > 2σ(I)] reflections	23089, 2250, 2102	17172, 5672, 5585	46739, 12843, 10448
R_{int}	0.028	0.023	0.029
(sin θ/λ)max (Å^{-1})	0.667	0.667	0.602
R[F^2 > 2σ(F^2)], wR(F^2), S	0.027, 0.074, 1.06	0.018, 0.046, 1.06	0.034, 0.103, 1.04
No. of reflections	2250	5672	12843
No. of parameters	118	271	901
No. of restraints		2	
$\Delta\rho_{max}$, $\Delta\rho_{min}$ (e Å^{-3})	0.46, –0.24	0.55, –0.27	0.68, –0.36

Table 2. Selected bond distances and angles for **4-PyCH$_2$OCS$_2$Na**, **[Py-Sn]**, and **[Py-Cu]**.

4-PyCH$_2$OCS$_2$Na				**[Py-Sn]**				**[Py-Cu]**			
Bonds	(Å)	Angles	(°)	Bonds	(Å)	Angles	(°)	Bonds	(Å)	Angles	(°)
Na1'''-N1	2.4682(11)	N1'-Na1'-O1	83.04(3)	Sn1-C31	2.128(3)	C31-Sn1-C11	119.25(11)	Cu1-P2A	2.2331(6)	P2A-Cu1-P1A	126.08(2)
Na1'-O2	2.4761(9)	O2-Na1'-O1	122.87(3)	Sn1-C11	2.136(3)	C31-Sn1-C21	116.62(11)	Cu1-P1A	2.2460(6)	P2A-Cu1-S1A	109.44(2)
Na1'-O1	2.5425(9)	N1'-Na1'-S1'	90.62(3)	Sn1-C21	2.143(3)	C11-Sn1-C21	122.87(11)	Cu1-S1A	2.3899(6)	P1A-Cu1-S1A	112.39(2)
Na1-S1	2.9306(6)	O2-Na1'-S1'	137.009(19)	Sn1-N1'	2.529(2)	C31-Sn1-N1'	89.81(9)	Cu1-S2A	2.4273(6)	P2A-Cu1-S2A	119.22(2)
Na1'-S1	2.9856(6)	O1-Na1'-S1'	87.52(2)	Sn1-S1	2.5932(7)	C11-Sn1-N1'	81.21(9)	Cu2-P2B	2.2307(6)	P1A-Cu1-S2A	103.28(2)
Na1''-S1	3.0301(5)	N1'-Na1'-S1	88.01(3)			C21-Sn1-N1'	88.08(9)	Cu2-P1B	2.2359(6)	S1A-Cu1-S2A	75.31(2)
Na1-S2	3.0357(6)	O2-Na1'-S1	74.025(18)			C31-Sn1-S1	99.70(8)	Cu2-S1B	2.3758(6)	P2B-Cu2-P1B	125.16(2)
Na1-Na1''	3.6763(9)	O1-Na1'-S1	53.968(19)			C11-Sn1-S1	83.90(8)	Cu2-S2B	2.4388(6)	P2B-Cu2-S1B	108.47(2)
		S1'-Na1'-S1	141.346(18)			C21-Sn1-S1	97.94(8)			P1B-Cu2-S1B	114.83(2)
		N1'-Na1'-S1''	166.66(3)			N1'-Sn1-S1	164.89(6)			P2B-Cu2-S2B	117.32(2)
		O1-Na1'-S1''	89.92(2)							P1B-Cu2-S2B	105.17(2)
		S1'-Na1'-S1''	77.725(13)							S1B-Cu2-S2B	75.31(2)
		S1-Na1'-S1''	97.016(14)								
		N1'-Na1'-S2	87.92(3)								
		O2-Na1'-S2'	89.59(2)								
		O1-Na1'-S2'	146.36(3)								
		S1-Na1-S2	60.163 (12)								
		S1-Na1'-S2'	158.148 (19)								
		S1-Na1''-S2'''	91.787 (14)								

References

[1] a) Cheng, C.; Stoddart, J. F. *ChemPhysChem* **2016**, *17*, 1780;

b) Fahrenbach, A. C.; Warren, S. C.; Incorvati, J. T.; Avestro, A.-J.; Barnes, J. C.; Stoddart, J. F.; Grzybowski, B. A. *Adv. Mater*. **2013**, *25*, 331;

c) Stang, P. J.; Saha, M. L.; Yan, X *Acc. Chem. Res*. **2016**, *49*, 2527;

d) Inokuma, Y.; Yoshioka, S.; Ariyoshi, J.; Arai, T.; Hitora, Y.; Takada, K.; Matsunaga, S.; Rissanen, K.; Fujita, M. *Nature* **2013**, *495*, 461;

e) Inokuma, Y.; Kawano, M.; Fujita, M. *Nat. Chem*. **2011**, *3*, 349;

f) Yoshizawa, M.; Fujita, M. *Pure Appl. Chem.* **2005***, 77*, 1107;

g) Liu, K.; Zhang, X.; Meng, X.; Shi, W.; Cheng, P.; Powell, A. K. *Chem. Soc. Rev*. **2016**, *45*, 2423;

h) Waldmann, O. *Coord. Chem. Rev.* **2005***, 249*, 2550.

[2] a) Leininger, S.; Olenyuk, B.; Stang, P. J. *Chem. Rev.* **2000***, 100*, 853;

b) Cook, T. R.; Stang, P. J. *Chem. Rev*. **2015**, *115*, 7001.

c) R. Chakrabarty, R.; Mukherjee, P. S.; Stang, P. J. *Chem. Rev.* **2011**, *111*, 6810.

d) Fujita, M.; Tominaga, M.; Hori, A.; Therrien, B. *Acc. Chem. Res.* **2005***, 38*, 369;

e) Roesky, H. W.; Andruh, M. *Coord. Chem. Rev.* **2003***, 236*, 91.

[3] a) Haiduc, I. *Appl. Organomet. Chem.* **2007***, 21*, 476;

b) Zukerman-Schpector, J.; Haiduc, I. *CrystEngComm* **2002***, 4*, 178;

c) Haiduc, I.; Zukerman-Schpector, J. *Phosphorus, Sulfur, Silicon Relat. Elem.* **2001***, 171-172*, 171;

d) Haiduc, I. *Coord. Chem. Rev.* **1997***, 158*, 325;

e) Tiekink, E. R. T. *CrystEngComm* **2006***, 8*, 104;

f) Tiekink, E. R. T. *CrystEngComm* **2003***, 5*, 101.

[4] a) Steiner, T. *Angew. Chem. Int. Ed.* **2002**, *41*, 48;

b) Hosseini, M. W. *Acc. Chem. Res.* **2005***, 38*, 313;

c) Beatty, A. M. *Coord. Chem. Rev.* **2003***, 246*, 131;

d) Braga, D.; Maini, L.; Polito, M.; Tagliavini, E.; Grepioni F. *Coord. Chem. Rev.* **2003***, 246*, 53.

[5] a) Claessens, C. G.; Stoddart, J. F. *J. Phys. Org. Chem.* **1997***, 10*, 254;

b) Janiak, C. *Dalton Trans.* **2000**, 3885;

c) Hunter, C. A.; Sanders, J. K. M. *J. Am. Chem. Soc.* **1990***, 120*, 5525;

d) Semeniuc, R. F.; Reamer, T. J.; Smith, M. D. *New J. Chem*. **2010**, *34*, 439.

[6] a) Li, L.; Fanna, D. J.; Shepherd, N. D.; Lindoy, L. F.; Li, F. *J. Incl. Phenom. Macrocycl. Chem.* **2015**, *82*, 3;

b) Kumar, G.; Gupta, R. *Chem. Soc. Rev.* **2013**, *42*, 9403;

c) Das, M. C.; Xiang, S.; Zhang, Z.; Chen, B. *Angew. Chem. Int. Ed.* **2011**, *50*, 10510;

[7] a) Vollmer, M. V.; Xie, J.; Lu, C. C. *J. Am. Chem. Soc*. **2017**, *139*, 6570;

b) Alexandru, M.-G.; Visinescu, D.; Shova, S.; Andruh, M.; Lloret, F.; Julve, M. *Inorg. Chem.* **2017**, *56*, 2258;

c) Visinescu, D.; Alexandru, M.-G.; Madalan, A. M.; Jeon, I.-R.; Mathoniere, C.; Clerac, R.; Andruh, M. *Dalton Trans*. **2016**, *45*, 7642;

d) Henderson, W.; Nicholson, B. K.; Fortney-Zirker, R. G.; Patel, S.; Lane, J. R.; Wyllie, M. J.; Tiekink, E.R. T. *Inorg. Chim. Acta* **2015**, *425*, 154;

e) Andruh, M.; Costes, J.-P.; Diaz, C.; Gao, S. *Inorg. Chem*. **2009**, *48*, 3342;

f) Rose, S. L.; Henderson, W.; Nicholson, B. K.; Hor, T. S. A. *Inorg. Chim. Acta* **2009**, *362*, 5237;

g) Garibay, S. J.; Stork, J. R.; Cohen, S. M. *Prog. Inorg. Chem*. **2009**, *56*, 335;

h) Soerensen, M. A.; Weihe, H.; Vinum, M. G.; Mortensen, J. S.; Doerrer, L. H.; Bendix, J. Chem. Sci. 2017, 8, 3566.

[8] a) Andruh, M. *Chem. Commun*. 2007, 2565;

b) Champness, N. R. *Dalton Trans.* 2006, 877;

c) Wuest, J. D. *Chem. Commun.* 2005, 5830;

d) Biradha, K.; Sarkar, M.; Rajput, L. *Chem. Commun.* 2006, 4169.

[9] a) Winter, G. *Rev. Inorg. Chem.* **1980***, 2*, 253;

b) Tiekink, E. R. T.; Winter, G. *Rev. Inorg. Chem.* **1992***, 12*, 183;

c) Haiduc, I.; Sowerby, D. B.; Lu, S.-F. *Polyhedron* **1995***, 14*, 3389;

d) Haiduc, I.; Sowerby, D. B. *Polyhedron* **1996***, 15*, 2469;

e) Garje, S. S.; Jain, V. K. *Coord. Chem. Rev.* **2003***, 236*, 35.

f) Tiekink, E. R. T.; Haiduc, I. *Prog. Inorg. Chem.* **2005***, 54*, 127.

[10] a) M. E. Padilla-Tosta, O. D. Fox, M. G. B. Drew, P. D. Beer, Angew. Chem. Int. Ed. 2001, 40, 4235;

b) P. D. Beer, N. Berry, M. G. B. Drew, O. D. Fox, M. E. Padilla-Tosta, S. Patell, Chem. Commun. 2001, 199;

c) P. D. Beer, A. G. Cheetham, M. G. B. Drew, O. D. Fox, E. J. Hayes, T. D. Rolls, Dalton Trans. 2003, 603;

d) W. W. H. Wong, D. Curiel, A. R. Cowley, P. D. Beer, Dalton Trans. 2005, 359;

e) W. W. H. Wong, D. Curiel, S.-W. Lai, M. G. B. Drew, P. D. Beer, Dalton Trans. 2005, 774;

f) J. Cookson, P. D. Beer, Dalton Trans. 2007, 1459.

[11] a) M. J. Macgregor, G. Hogarth, A. L. Thompson, J. D. E. T. Wilton-Ely, Organometallics 2009, 28, 197;
b) S. Naeem, A. J. P. White, G. Hogarth, J. D. E. T. Wilton-Ely, Organometallics 2010, 29, 2547.

[12] R. Reyes-Martínez, P. García y García, M. López-Cardoso, H. Höpfl, H. Tlahuext, Dalton Trans. 2008, 6624.

[13] a) Hoskins, B. F.; Pannan, C. D. *Chem. Commun*. **1975**, 408;
d) Dakternieks, D.; Di Giacomo, R.; Gable, R. W.; Hoskins, B. F. *J. Am. Chem. Soc.* **1988***, 110*, 6753.

[14] Krebs, H; Weber, E. F.; Fassbender, H. *Z. Anorg. Allg. Chem.* **1954***, 276*, 128.

[15] Semeniuc, R. F.; Reamer, T. J.; Blitz, J. P.; Wheeler, K. A.; Smith, M. D. *Inorg. Chem.* **2010**, *49*, 2624.

[16] Addison, A. W.; Nageswara R. T.; Reedijk, J; van Rijn, J.; Verschoor, G. C. *J. Chem. Soc. Dalton Trans.* **1984**, 1349.

[17] Berry, J. F. *Dalton Trans*., **2012**, *41*, 700.

[18] F. A. Cotton, E. A. Hillard and C. A.Murillo, *J. Am. Chem. Soc.*, **2002**, *124*, 5658.

[19] Yoe, J. H.; Jones, A. L. *Anal. Chem*. **1944**, *16*, 111.

[20] Cotton, F. A.; Goodgame, D. M. L. *J. Chem. Soc*. 1960, 5267.

[21] Rempel, G. A.; Legzdins, P.; Smith, H.; Wilkinson, G. *Inorg. Synth.* **1972**, *13*, 90.

[22] SMART Version 5.630, SAINT+ Version 6.45 and SADABS Version 2.10. Bruker Analytical X-ray Systems, Inc., Madison, Wisconsin, USA, 2003.

[23] Sheldrick, G. M. SHELXTL Version 6.14; Bruker Analytical X-ray Systems, Inc., Madison, Wisconsin, USA, 2000.

[24] Barbour, L. J. *J. Supramol. Chem.* **2001**, *1*, 189.

[25] Sheldrick, G. M. *Acta Crystallogr., Sect. A* **2008**, *64*, 112.

Graphical Abstract

Tetrametallic heteronuclear complexes were prepared from neutral metalloligands, comprising of a second-generation xanthate ligand coordinated to Sn(IV) and Cu(I) centers.

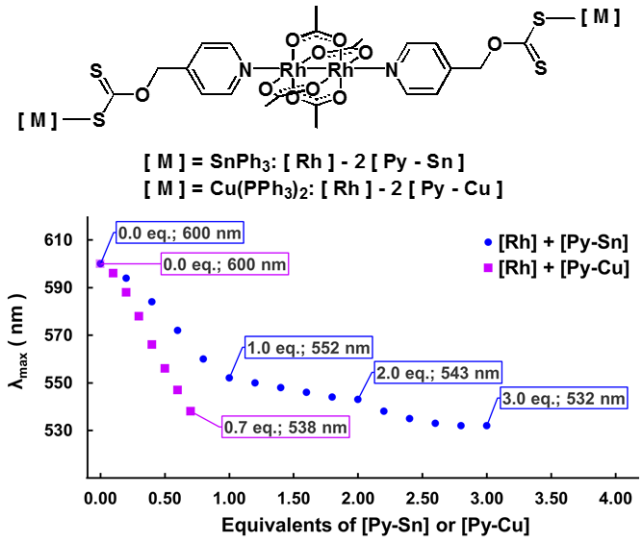

Highlights:

- A backbone functionalized xanthate ligand has been prepared.
- Its propensity to coordinate to Sn(IV) and Cu(I) centers has been explored.
- Neutral metalloligands have been obtained.
- Hetero-tetrametallic complexes have been prepared.